



Nuclear Regulatory Commission
 Exhibit # - PWA000006-00-BD01
 Docket # - 05000293
 Identified: 02/22/2011

Admitted: 02/22/2011
 Rejected:

Withdrawn:
 Stricken:

PWA 00006
 Pilgrim LR Proceeding
 50-293-LR, 06-848-02-LR

JANUARY 2006

ANGEVINE ET AL.

137

PWA-Angevine- Pollutant transport - New England's Coast

Modeling of the Coastal Boundary Layer and Pollutant Transport in New England

WAYNE M. ANGEVINE

Cooperative Institute for Research in Environmental Sciences and NOAA/Aeronomy Laboratory, Boulder, Colorado

MICHAEL TJERNSTRÖM AND MARK ŽAGAR*

Meteorological Institute, University of Stockholm, Stockholm, Sweden

(Manuscript 1 February 2005, in final form 14 June 2005)

ABSTRACT

Concentrations of ozone exceeding regulatory standards are regularly observed along the coasts of New Hampshire and Maine in summer. These events are primarily caused by the transport of pollutants from urban areas in Massachusetts and farther south and west. Pollutant transport is most efficient over the ocean. The coastline makes transport processes complex because it makes the structure of the atmospheric boundary layer complex. During pollution episodes, the air over land in daytime is warmer than the sea surface, so air transported from land over water becomes statically stable and the formerly well-mixed boundary layer separates into possibly several layers, each transported in a different direction. This study examines several of the atmospheric boundary layer processes involved in pollutant transport. A three-dimensional model [the Coupled Ocean–Atmosphere Mesoscale Prediction System (COAMPS)] run on grids of 2.5 and 7.5 km is used to examine the winds, thermodynamic structure, and structure of tracer plumes emitted from Boston, Massachusetts, and New York City, New York, in two different real cases—one dominated by large-scale transport (22–23 July 2002) and one with important mesoscale effects (11–14 August 2002). The model simulations are compared with measurements taken during the 2002 New England Air Quality Study. The model simulates the basic structure of the two different episodes well. The boundary layer stability over the cold water is weaker in the model than in reality. The tracer allows for easy visualization of the pollutant transport.

1. Introduction

A coastline poses significant problems for understanding, monitoring, and forecasting the transport and dispersion of pollutants in the atmosphere. At the same time, coastal areas are often highly populated, and the consequences of pollution emissions and transport are important. The coastline constitutes an abrupt change in all surface parameters, such as roughness, temperature, and terrain height. The responses in the lower atmosphere—the boundary layer (BL)—are complex and diverse.

The most commonly known resulting phenomena are

* Current affiliation: Environmental Agency of Slovenia, Meteorological Office, Ljubljana, Slovenia.

Corresponding author address: Wayne M. Angevine, NOAA/Aeronomy Lab R/AL3, 325 Broadway, Boulder, CO 80305.
 E-mail: Wayne.M.Angevine@noaa.gov

the sea breeze and the formation of offshore internal boundary layers. The sea breeze is the prototypical mesoscale circulation and was the first to be simulated in numerical models (cf. e.g., Estoque 1961). With the development of more advanced models, it has been revisited many times (e.g., Colby 2004; Marshall et al. 2004). Given the effort invested, one might think that almost all there is to know would be known by now. However, although the theoretical background is well understood and is simple enough, real sea breezes are very sensitive to real environmental complexity, such as variations in coastline orientation and coastal terrain, surface temperature, and the background (larger scale) flow.

Coastal northern New England receives pollutants transported from more populous areas, which cause concentrations of ozone to exceed national standards several times every summer. Unlike the classical pollution situation, where pollutants are emitted into a stagnant air mass and primarily affect an urban area or a compact region, the events affecting coastal New

Hampshire and Maine are almost entirely because of transport from sources at 50–500-km distances. The marine atmospheric boundary layer provides for efficient transport. Because of the relatively cold water, offshore transport occurs in stable layers. To understand these pollution episodes, we need to understand the complex four-dimensional structure of the coastal boundary layer. Furthermore, longer-range transport of pollutants to the North Atlantic and even Europe also occurs (Cooper and Parrish 2004) and is modulated by the coastal and marine boundary layers.

Many studies have addressed pollutant transport on the urban scale or on the regional scale over land, but few have looked at regional-scale transport over coastal areas. Several studies of the region of Lake Michigan are notable exceptions (Lyons and Olsson 1973; Lyons and Cole 1976; Keen and Lyons 1978; Sillman et al. 1993; Dye et al. 1995; Fast and Heilman 2003). Sillman et al. (1993) also simulated a New England case.

In an earlier paper, Angevine et al. (2004) used measurements from the 2002 New England Air Quality Study (NEAQS) to describe the coastal transport situation. The measurements included chemistry and meteorology at the surface, and vertical profiles of wind, temperature, humidity, ozone, and aerosol backscatter. Even such a comprehensive suite of measurements, however, cannot completely determine the full four-dimensional structure of the coastal boundary layer. Therefore, we have undertaken a modeling study to further elucidate that structure and evolution.

The basic questions that we are interested in are the following ones.

- How quickly does the boundary layer stabilize after crossing from land to water? What fluxes are required to accomplish the stabilization?
- What physical processes create the surface-based inversion? Is shear-driven turbulence sufficient or does advected turbulence also play a role? How intense is the turbulence?
- Are multiple distinct layers formed from the continental boundary layer after it passes over the water, and if so, how many and how deep is each of the layers?
- Under what conditions is part of the polluted continental air lofted above a clean marine layer?
- Does a mixed layer form again downwind and, if so, how far downwind?
- What is the structure of the pollution plume from the continent in three dimensions? How does it vary with time?

This study utilizes a numerical model as its main tool to understand the relevant physical processes observed

during NEAQS. The model we use, the Coupled Ocean–Atmosphere Mesoscale Prediction System (COAMPS), is widely utilized both as a forecast model and in different science applications, as reported in a multitude of papers (cf. e.g., Haack et al. 2005, 2001; Skillingstad et al. 2005; Burk and Thompson 2004; Shi et al. 2004; Burk et al. 2003; Hanna and Yang 2001; Dorman et al. 2000; Burk and Haack 2000; Nachamkin 2004). Although this is not a model evaluation study, we examine how faithfully the models reproduce the measured state of the atmosphere where measurements are available. Where the model results differ from the measurements, we evaluate the causes and consequences of those deviations. An extensive model evaluation is, however, beyond the scope of this paper.

2. Model and case studies

a. COAMPS model

Three-dimensional numerical simulations were performed with version 2 of the COAMPS atmospheric model, developed at the U.S. Naval Research Laboratory in Monterey, California (Hodur 1997). This is a nonhydrostatic primitive equation compressible Boussinesq model with a terrain-following vertical coordinate. Turbulent kinetic energy (TKE) is prognostic and provides input to the “level 2.5” turbulence closure in the hierarchy of closures by Mellor and Yamada (1974). The diabatic part of the model includes explicit moist physics (Rutledge and Hobbs 1983) while subgrid convection at model resolutions greater than ~ 10 km is parameterized using a version of the Kain–Fritsch scheme (Kain and Fritsch 1993). At very high resolution COAMPS effectively becomes a cloud-resolving model. Radiation is treated as in Harshvardhan et al. (1987). The ground surface temperature and soil moisture are computed using a force-restore scheme, taking into account different land classes with predefined albedo (for a snow-free surface). Land-use data were from the U.S. Geological Survey database at 1-km resolution and terrain height was from the U.S. National Imagery and Mapping Agency Digital Terrain Elevation Data level 0, also at 1-km resolution. For ocean surfaces, the sea surface temperature (SST) was prescribed from European Centre for Medium-Range Weather Forecasts (ECMWF) analyses. Consecutive static nesting was used with successive grids at 67.5-, 22.5-, 7.5-, and 2.5-km horizontal resolution (Fig. 1). The vertical resolution did not change between the nests. Forty vertical levels were used in the simulations, most densely distributed in the planetary boundary layer (13 levels within the lowest 1 km, 5 levels within

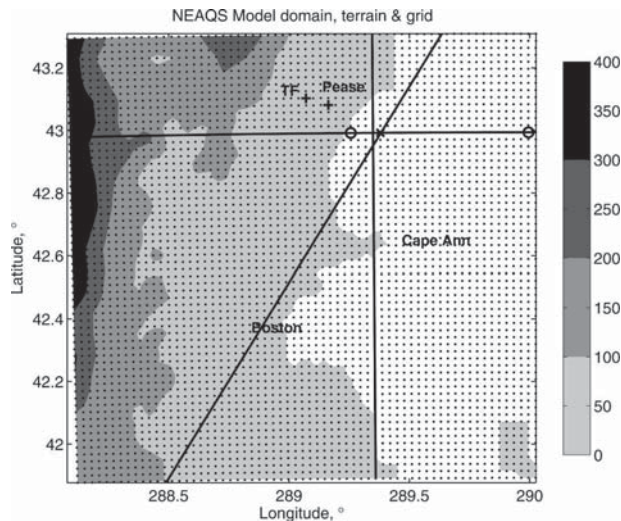


FIG. 1. Innermost model domain showing terrain (shaded, m MSL), grid (dots), cross-sectional lines, and locations of interest: Thompson Farm (TF) (+), Pease (+), Appledore Island (x), near-shore point (o), and offshore point (o). Cape Ann and the general location of Boston are also labeled.

lowest 100 m, and the 2 lowest levels at 1 and 5 m above the surface).

The model is initialized from an operational ECMWF analysis. Lateral boundary conditions are applied using the Davies relaxation scheme (Davies 1976), updated 6 hourly, also using operational analyses from ECMWF. This procedure means that the simulations performed here are strictly speaking not forecasts. Instead, we force the outer domain of COAMPS by the best available representation of the three-dimensional structure of the atmosphere (from the ECMWF analysis). COAMPS is then used as an advanced interpretation tool to generate four-dimensional representations (space and time) of the dynamic fields of the atmosphere at a much higher spatial scale, through the successive nesting. No observations were assimilated in COAMPS; assimilation of observations is inherited from the ECMWF assimilation cycle (ECMWF utilize 4D variational data assimilation; see additional information online at <http://www.ecmwf.org>). Beyond the spinup of the model physics, taking place during the first <6 h of simulation, COAMPS produces an internally consistent solution at the higher resolution. Remaining errors are then determined either by systematic errors in COAMPS or by errors in the ECMWF analyses and do not necessarily grow with time. This procedure also means that special observations from NEAQS are truly independent.

A tracer was emitted from the Boston, Massachusetts, area in the 2.5-km grid spacing runs, and sepa-

rately from both Boston and New York City (NYC), New York, in the 7.5-km runs. The tracer provides a means of visualizing the general pattern of pollution transport from those sources, but is not intended to simulate absolute concentrations of any particular pollutant. The tracer was emitted in the three lowest model levels (at 1, 5, and 17 m AGL) at the constant rate of two units per time step over the most dense part of the urban area, and at one unit per time step in a ring of a 1×1 grid box around that area. Because New York City is considerably larger in area than Boston, the tracer emissions are in the ratio of 76/14. In other words, New York City emits about 5.5 times as much tracer as does Boston. The tracers in our simulation are treated as passive substances, meaning that they are subject to advection and mixing but are neither deposited nor chemically transforming. The advection scheme for tracer in COAMPS is Bott's fifth-order flux-form advection with area preservation and positiveness (Bott 1989, 1992). This capability has been used in several other studies, for example, Liu et al. (2003).

b. Description of cases

Two contrasting pollution episodes occurred during the summer of 2002 in northern New England. On 22–23 July, a moderate southwesterly wind brought pollutants to coastal New Hampshire and Maine from Boston and the urban areas farther south along the U.S. east coast. The situation was dominated by the large-scale flow. In contrast, an extended episode in mid-August occurred under lighter synoptic forcing, allowing mesoscale effects such as the sea breeze to play a more important role. These two episodes were discussed from the observational perspective by Angevine et al. (2004). Here we use COAMPS to illuminate the boundary layer transport issues during those episodes. For the July results shown, the model was initialized at 0000 UTC 21 July (1900 EST 20 July). For the August case, initialization was at 1200 UTC (0700 EST) 11 August.

3. Winds

A model evaluation is beyond the scope of the present paper, but in order to have confidence in model results for specific cases, we must verify that they correspond, at least in their key features, to the real situation. Before discussing the model winds in detail, we therefore present a few of the many comparisons we have carried out to that end. The model winds are compared with winds measured by the radar wind profiler at Pease International Tradeport (see Fig. 1), near Portsmouth, New Hampshire, in Figs. 2 and 3. On

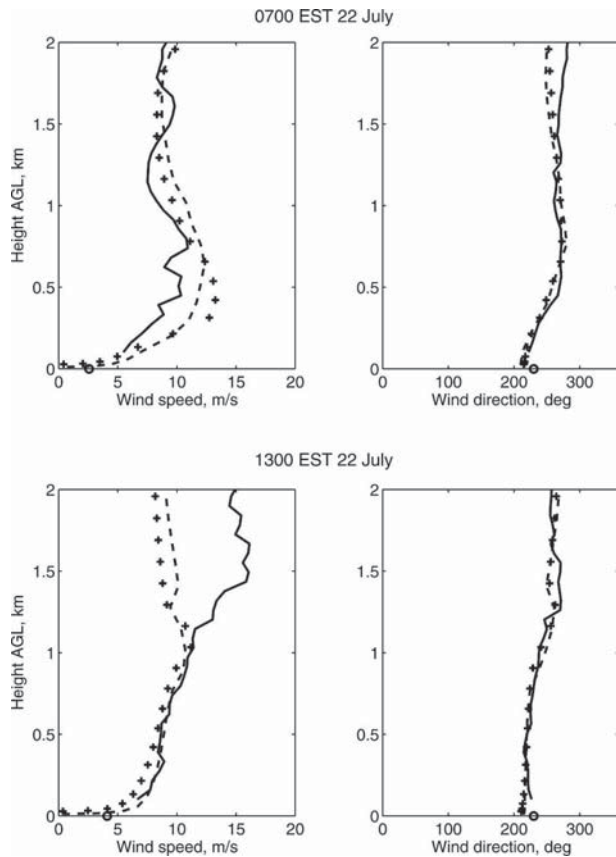


FIG. 2. Profiles of wind over the Pease site (see Fig. 1) at two times on 22 Jul; observation from radar wind profiler (solid line), surface observation (circle), model output at 2.5-km grid spacing (dashed line), and model output at 7.5-km grid spacing (plus symbols).

22 July, the model agrees very well with the measured winds in the morning. At midday, the winds below 1 km also agree very well, but the modeled wind speed aloft is lower than that observed. At both times, the 2.5-km winds are a little closer to the observations than the winds on the 7.5-km grid. On 13 August (Fig. 3), there are somewhat larger differences between the model and observations. A difference in wind direction near the surface at night that, at first glance, appears large, occurs at a very low speed. The model does produce lower speeds at midday both below 500 m and above 1 km, which could have some impact on pollutant transport.

The top panels of Fig. 4 show horizontal cross sections of the low-level (~ 50 m) winds in the morning and near midday of 22 July. No sea breeze develops, but there is a subtle shift to more southerly winds offshore, and some increase in speed. This may be the geostrophically balanced response to the east–west temperature gradient when the background flow is strong

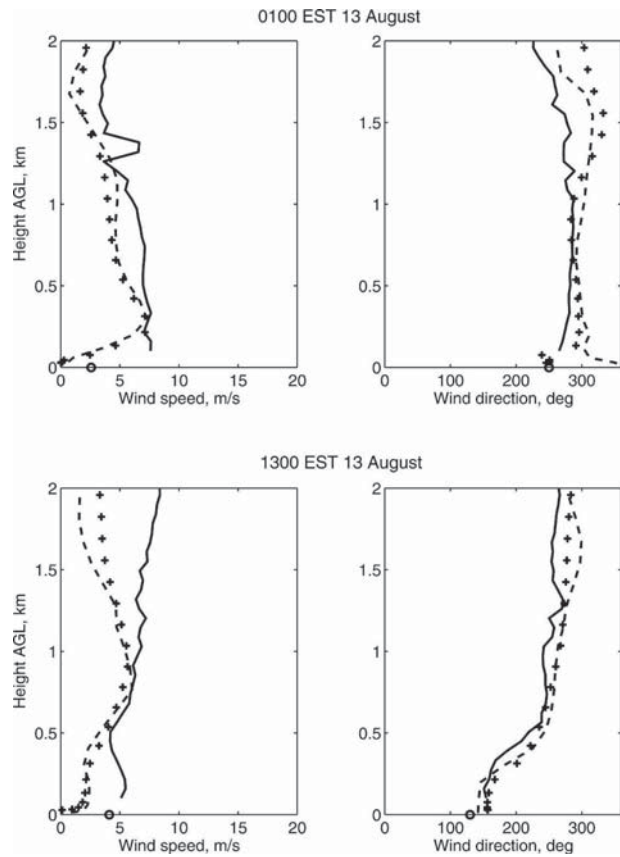


FIG. 3. Profiles of wind over the Pease site (see Fig. 1) at two times on 13 Aug; observation from radar wind profiler (solid line), surface observation (circle), model output at 2.5-km grid spacing (dashed line), and model output at 7.5-km grid spacing (plus symbols).

enough to prevent the formation of a proper sea breeze. The flow at inland locations decelerates from morning to afternoon, and there is a tongue of slower flow north of Cape Ann (the prominent cape in the middle of the figure). Vertical cross sections of the cross-coast wind component (lower panels of Fig. 4) show that the offshore flow is decelerated offshore in the lowest few hundred meters. The vertical winds (not shown) show low-level convergence just offshore.

In contrast, the sea breeze dominates the winds on 13 August, as shown in Fig. 5. The background flow is weaker. The horizontal cross sections (top panels) actually show two sea-breeze systems, separated by Cape Ann, and the effect of the local coastline geometry is obvious. The sea breeze south of Cape Ann is slightly stronger than that north of Cape Ann. The sea-breeze front is marked quite clearly by an almost zero wind speed band inland, and is also implied by an up–down couplet in the vertical winds and by the TKE pattern (not shown). The circulation on the 12th (not shown) is

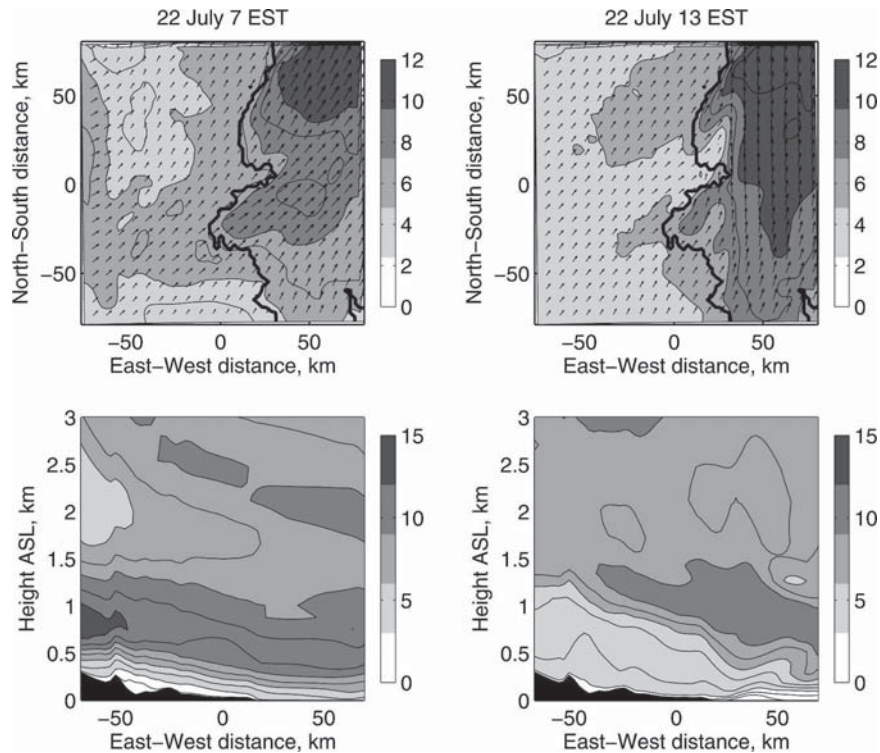


FIG. 4. (top) Model winds at approximately 50 m above ground level [vectors; speed (m s^{-1}) is shaded] for two times on 22 Jul. (bottom) Vertical cross section of east-west wind component along the east-west line shown in Fig. 1 for the same times.

very similar. Vertical cross sections of the cross-coast wind component (lower panels) also clearly show the sea breeze, with an anvil-shaped front. The inland convectively heated layer is about 1.5 km deep but the sea breeze is only 200–300 m deep, except at the front where it rises to about 500 m. The offshore flow aloft is skewed and resembles a gravity wave rather than the traditional return flow. The wavelike feature is also implied by the temperature field (not shown), as a warm trough tilting inland with height, and in the vertical wind speed (Fig. 6), where it seems that the up-down couplet associated with the front triggers a wave motion propagating offshore with height.

The dominant feature during the night is the strong offshore flow jet that starts after the sea breeze stops. The right panels of Fig. 5 show relatively strong winds offshore with local maxima on either side of Cape Ann, where the two lobes of the sea-breeze system were previously located. Analyzing different times shows the strong winds forming over land and propagating downwind with time. This, and the location of the local maxima on either side of Cape Ann, indicates that this flow starts as an inertial oscillation response, initiated as the opposing flow of the sea breeze comes to an end.

The sea-breeze circulations in this August episode

extend almost to the seaward edge of the inner domain of the model. For example, at 1400 LST 13 August the cross-coast wind speed near the surface approaches zero at approximately 60–80 km from the sea-breeze front, depending on the exact location, close to the boundary of the innermost nest. This size is roughly consistent with a shallow-water Rossby radius of deformation of about ~ 80 km, based on a ~ 200 -m-deep layer capped by a $\sim 10^\circ\text{C}$ inversion, as was simulated far away from the coast. The Rossby radius indicates the maximum expected extent of a sea breeze, because it is an example of a geostrophic adjustment on the meso-scale.

Figures 7 and 8 show time–height cross sections of the cross-coast wind component for the two cases. The July episode starts with onshore low-level flow on the 21st, but for the rest of the episode the flow never reverses, although there is a diurnal reduction in the flow indicating a sea-breeze-like component superimposed on the stronger background flow. There are strong nocturnal jets with an offshore component. Nocturnal jets were observed by a lidar on the coast at Rye Harbor, New Hampshire, a few kilometers south of Portsmouth (R. Banta 2004, personal communication). On the afternoon of 23 July, there is a strong

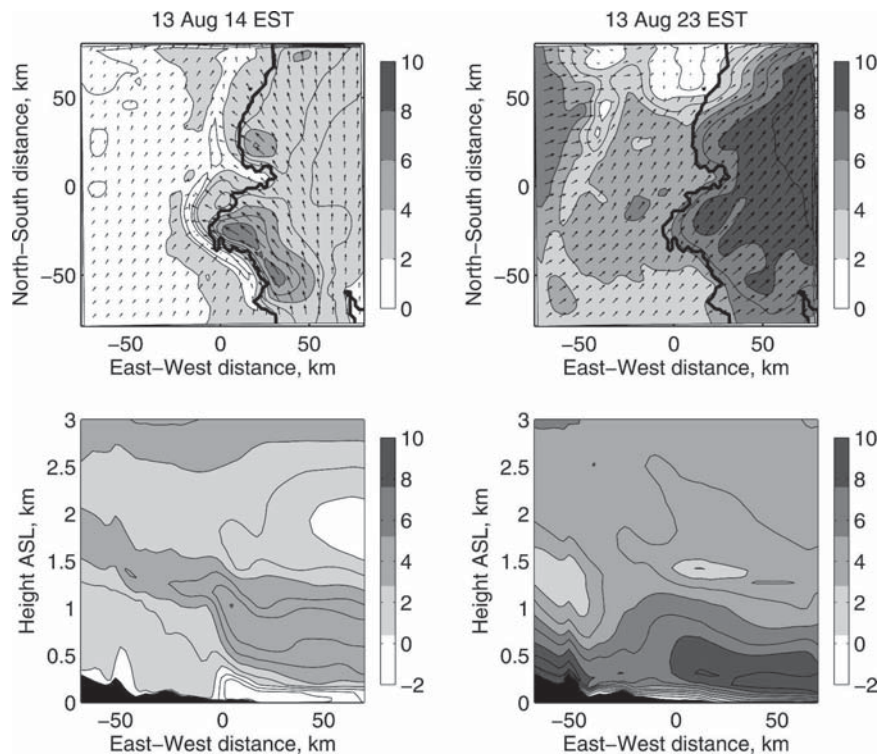


FIG. 5. (top) Model winds at approximately 50 m above ground level [vectors; speed (m s^{-1}) is shaded] for two times on 13 Aug. (bottom) Vertical cross section of east-west wind component along the east-west line shown in Fig. 1 for the same times.

frontal passage, ending the pollution episode. After the frontal passage, the model has northeasterly winds, but the observed winds are northwesterly, decreasing in speed and eventually becoming northeasterly by 1000 LST on 24 July.

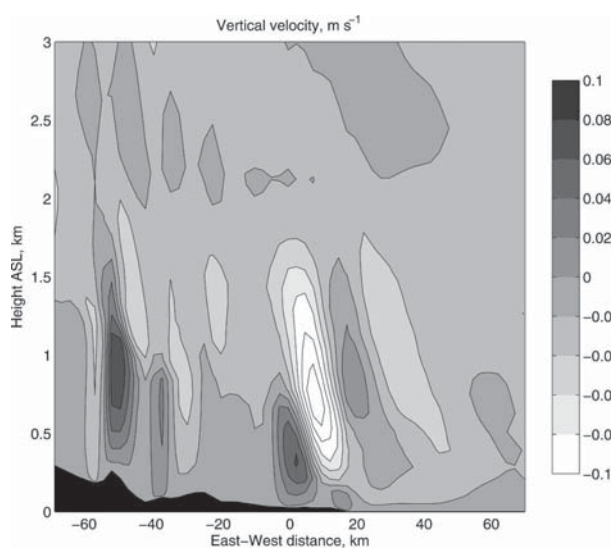


FIG. 6. Cross section of vertical velocity along the east-west line shown in Fig. 1 at 1300 LST 13 Jul.

The time-height cross sections for the August episode (Fig. 8) show the obvious sea breeze, which begins at about 1000 LST and continues until about 1800 LST. It is slightly weaker, starts later, and hardly penetrates

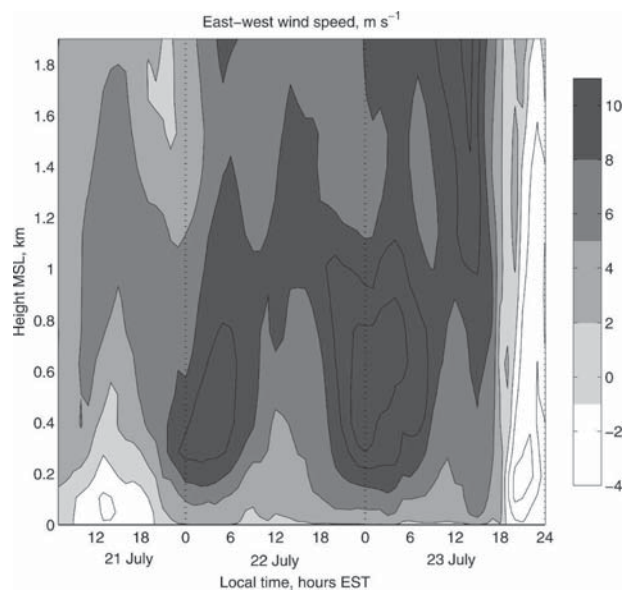


FIG. 7. Time-height cross section of east-west wind on 21–23 Jul at the near-shore point shown in Fig. 1.

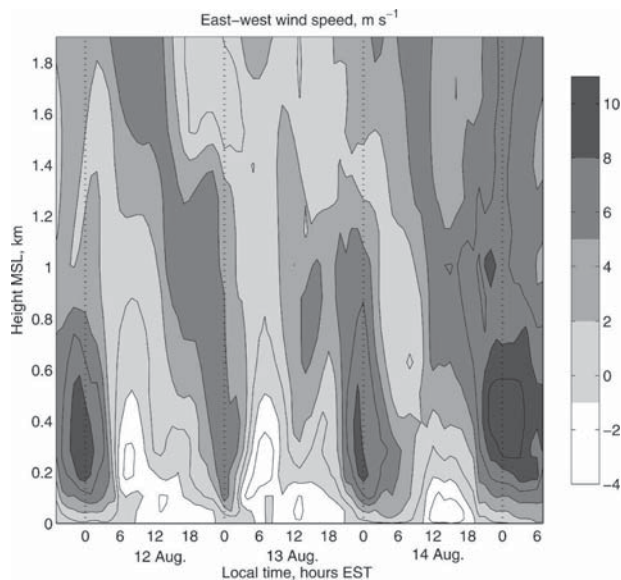


FIG. 8. Time–height cross section of east–west wind on 11–14 Aug at the near-shore point shown in Fig. 1.

inland at all on the 14th. This different behavior is probably explained by small changes in the synoptic flow patterns. On the 15th no sea breeze occurs, likely because the large-scale offshore flow is stronger.

Figure 8 also shows a diurnal cycle in the vertical structure of the cross-coast wind speed. On all 3 days, a period of near-zero offshore flow begins at about 2 km a few hours after midnight and descends to between 200 m and 1 km in the early morning, with maximum vertical extent at around 0600 LST. As the sea breeze develops, the low-speed period is replaced by a branch of enhanced offshore flow of a similar spatiotemporal structure, also starting about 2 km in the middle of the day and descending to the surface following the end of the sea breeze, forming an intense off-coast-flowing jet. The jet, previously described in the context of Fig. 5, has its maximum around midnight and is then followed by the next day’s early morning low-speed period.

4. Thermal structure and turbulence

The boundary layer over land undergoes the usual diurnal cycle during these episodes. The boundary layer over the water, by contrast, is always statically stable, but the details of the stable temperature profile vary with location and time of day. Figure 9 shows a comparison of potential temperature profiles from radio soundings launched from the National Oceanic and Atmospheric Administration (NOAA) Research Vessel (R/V) *Ronald H. Brown* with profiles from the 2.5-km grid model. The ship was moving in the area generally

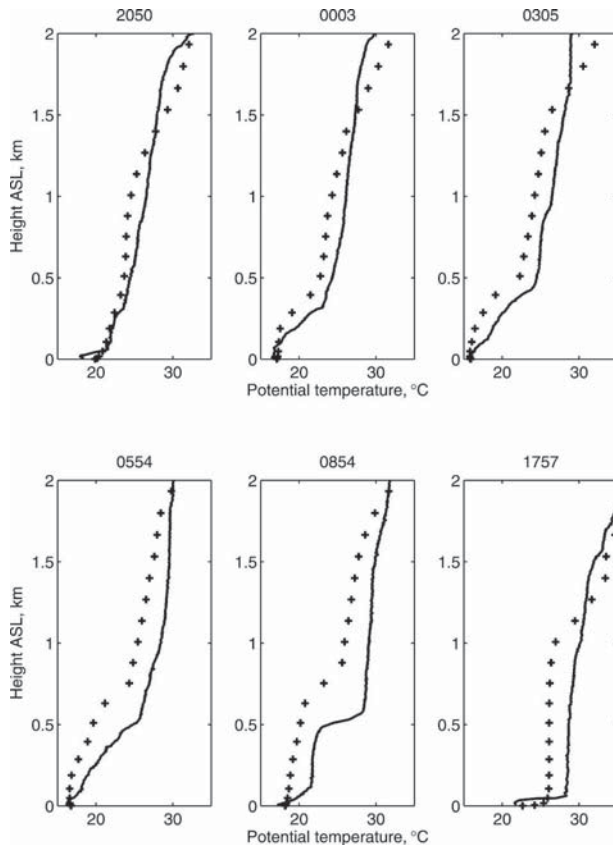


FIG. 9. Potential temperature profiles from rawinsondes (solid) and the model (plus symbols) at six times on 21 and 22 Jul. Times are listed above each panel in LST. Soundings were launched from the ship at various locations between Cape Ann and Appledore Island.

bounded by Cape Ann, the Isles of Shoals, and the northern Massachusetts–New Hampshire coast. The comparisons are made at the nearest model grid point to the ship location at the sounding launch time. The six soundings capture an entire diurnal cycle starting in the evening of 21 July. Most of the diurnal temperature change happens below 500 m. In the evening (between 2050 and 0305 LST), the observed and modeled temperatures decrease near the surface first and most strongly, with the temperature decrease propagating upward. This is a consequence of the gradual development of the stable boundary layer over the land. By sunrise (roughly represented by the 0554 LST sounding), there is a stable layer 500 m deep with a potential temperature difference between the surface and 500 m of approximately 9° and a roughly linear slope. After sunrise, the land boundary layer warms quickly, and by the 0854 LST sounding there is a near-neutral layer between about 100 and 400 m, with the strongly stable marine boundary layer below and a sharp inversion

above. By afternoon, the sounding has an extremely statically stable marine boundary layer less than 100 m deep, topped by the near-neutral continental boundary layer extending up to at least 1 km. The cycle can then begin again. It is worth noting that the sea surface temperature does not change very much between the soundings (it varies between 16.5° and 17.5°C). The statically stable lowest layer extends below the lowest sounding level to the surface with a temperature decrease of several more degrees at the time of the daytime soundings (2050 LST 21 July and 1757 LST 22 July). This is confirmed by measurements of the difference between the air temperature measured at 15 m on the ship and the sea surface temperatures (not shown). All soundings taken in the Gulf of Maine in summer with offshore flow show surface-based statically stable layers.

The model follows the general features of the diurnal cycle, but moderates the temporal and vertical structure. It does not cool as quickly near the surface in the early evening. The model profiles are generally too neutral in the lowest layers, so it misses the strong surface-based static stability in the 0305, 0554, and 0854 LST soundings entirely. It does have a surface-based inversion at 1757 LST, but it is much too weak, and the continental layer above is too cool.

Another way of looking at the thermodynamic structure is presented in Figs. 10 and 11, which show modeled time–height cross sections of potential temperature over land (Pease), a few kilometers offshore (Appledore Island, Maine), and far offshore. The patterns at these three sites are generally representative of those types of locations. For the July case (Fig. 10), we see the expected structure over land: a well-mixed continental boundary layer on the two afternoons with southwesterly winds, and static stability at night. At Appledore Island, the advected continental BL is present above 100 m in the afternoons, but it lies atop a shallow statically stable marine layer. The nighttime temperature profiles are rather similar over land and water because the nighttime minimum temperature over land is similar to the sea surface temperature (by coincidence). Far offshore, the structure is similar but the surface-based layer is deeper. After the frontal passage late on 23 July the BL is near neutral at all sites because the air is cooler and the wind has an easterly (overwater) component.

In the August case (Fig. 11) the land site still shows a nearly textbook boundary layer but with some complication from the sea breeze. The growth of the stable nocturnal boundary layer is particularly clear on the first two nights. The sea breeze abruptly terminates the well-mixed layer in the afternoon. Over the water, the

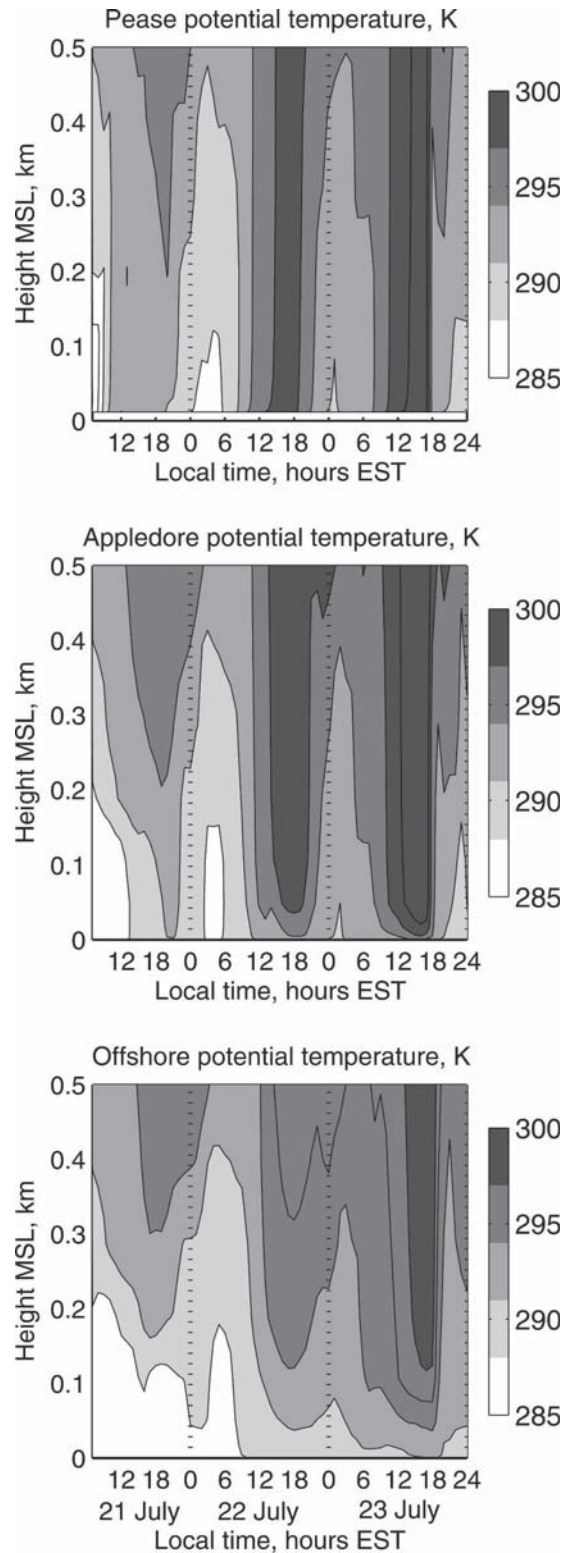


FIG. 10. Time–height cross sections of model potential temperature for 21–23 Jul over Pease, Appledore, and the offshore point.

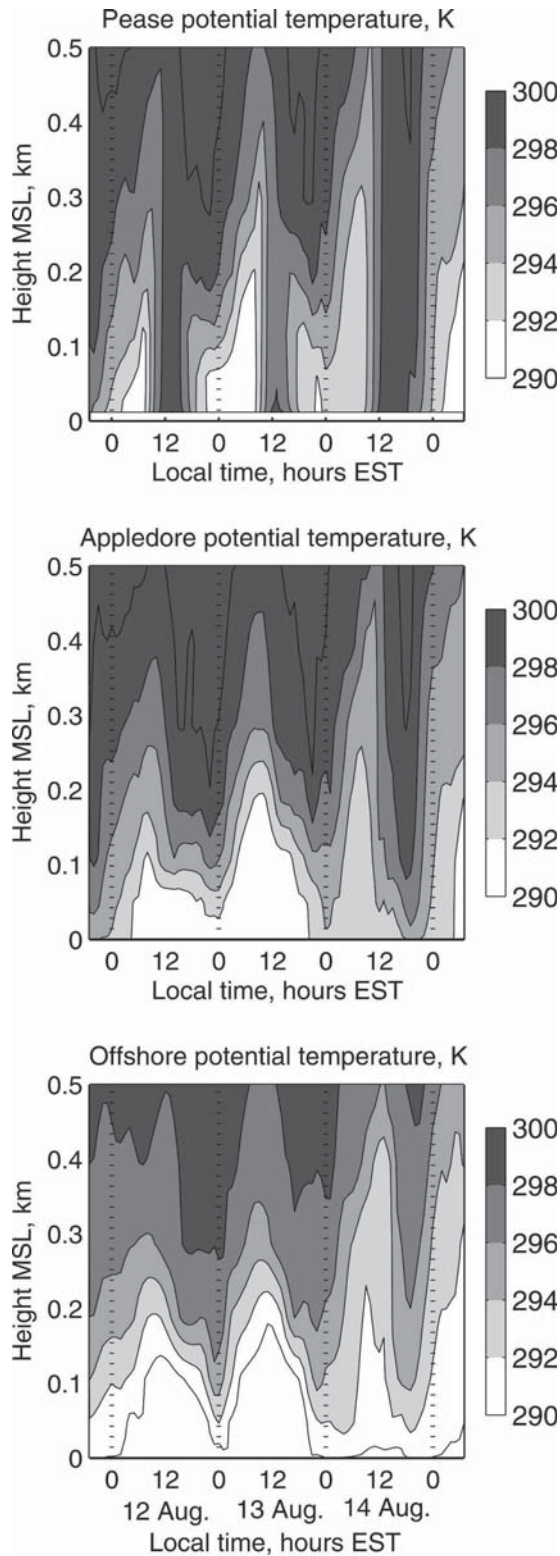


FIG. 11. Time–height cross sections of model potential temperature for 11–14 Aug over Pease, Appledore, and the offshore point.

profiles are always statically stable, but the potential temperature gradient near the surface is less in the mornings. The model actually produces a very shallow near-neutral layer close to the surface, as seen in Fig. 9, but the soundings suggest that this does not happen in reality. Far offshore the pattern is similar, but the surface temperatures are a little cooler and the layer affected by contact with the surface is deeper. It is clear that even this far from the coast, what happens at the coast has a significant effect. During the sea-breeze events, the scalar wind speed is at its minimum while the marine boundary layer depth is at a maximum (about 200 m). The scalar wind speed reaches its maximum in the strong offshore flow during the night, which is also when the vertical wind shear near the surface is the strongest. During these episodes, there is also significant shear above the jets.

The Richardson number diagnoses whether a layer will initiate, sustain, or damp turbulence. For purposes of this discussion we assume that gradient Richardson numbers less than 0.25 indicate active turbulence, values between 0.25 and 1 indicate a layer that may remain turbulent if it has a turbulent history, and values greater than 1 indicate turbulence will decay in layers. The contour levels in Figs. 12 and 13 are chosen accordingly. For both July and August cases over land, a deep turbulent layer is modeled during the day, although the early cutoff of turbulence by the sea breeze is quite visible in the August case (Fig. 12). Over water but relatively near shore (Appledore Island) in the July case (Fig. 11) the atmosphere should be able to sustain advected turbulence up to at least 500 m most of the time, and has actively turbulent regions from the surface to 200–300 m at night when the static stability is relaxed. An actively turbulent layer aloft also occurs on the evening of 22 July above the low-level jet. In the August case the background wind is weaker, and so active turbulence is confined to very near the surface and even advected turbulence is unlikely above 100 m during the day, except on the last day after the wind strength has increased. At night, the enhanced wind speed in the jets and the relaxation of static stability resulting from cooling over the land result in deeper layers that can support turbulence. The far-offshore Richardson number patterns are similar to those at Appledore Island, but the region of active turbulence is slightly deeper and more persistent in the July case (Fig. 11).

COAMPS predicts TKE and uses it to determine the amount of vertical mixing. We can use TKE to explore how the boundary layer structure is formed and maintained in the model. Figures 14 and 15 show TKE and potential temperature in the morning and at midday of

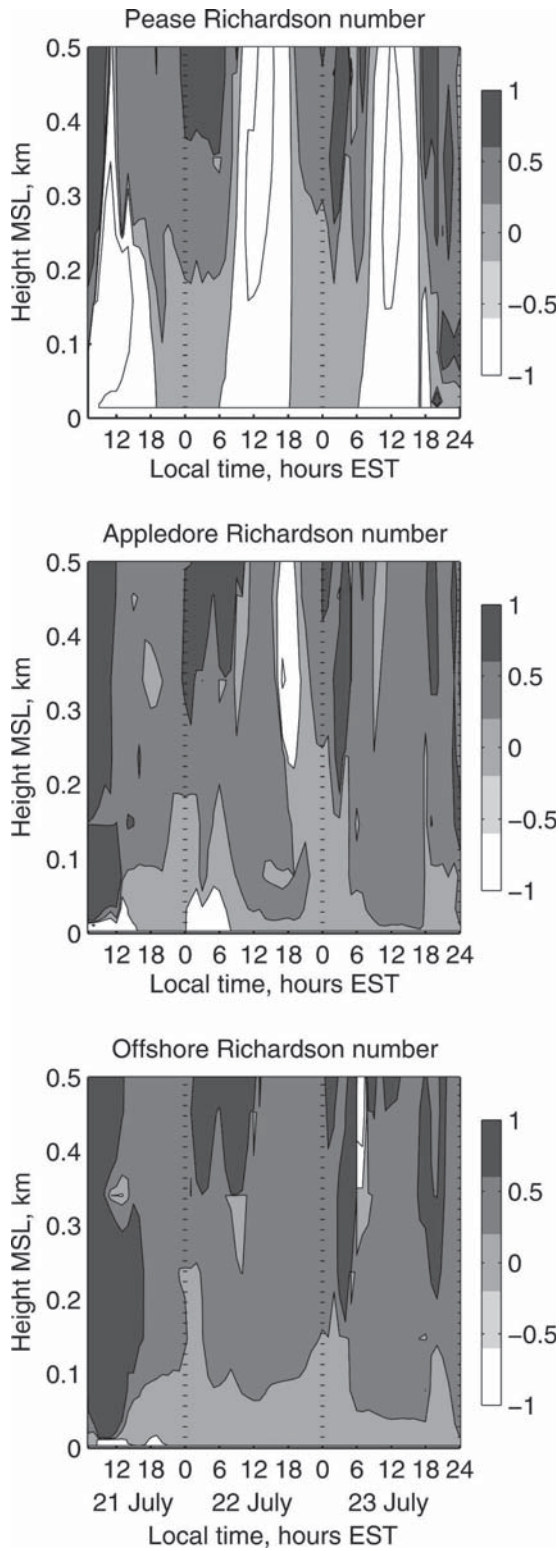


FIG. 12. Time–height cross sections of model Richardson number for 21–23 Jul over Pease, Appledore, and the offshore point. Contour levels are -1 , 0 , 0.25 , and 1 .

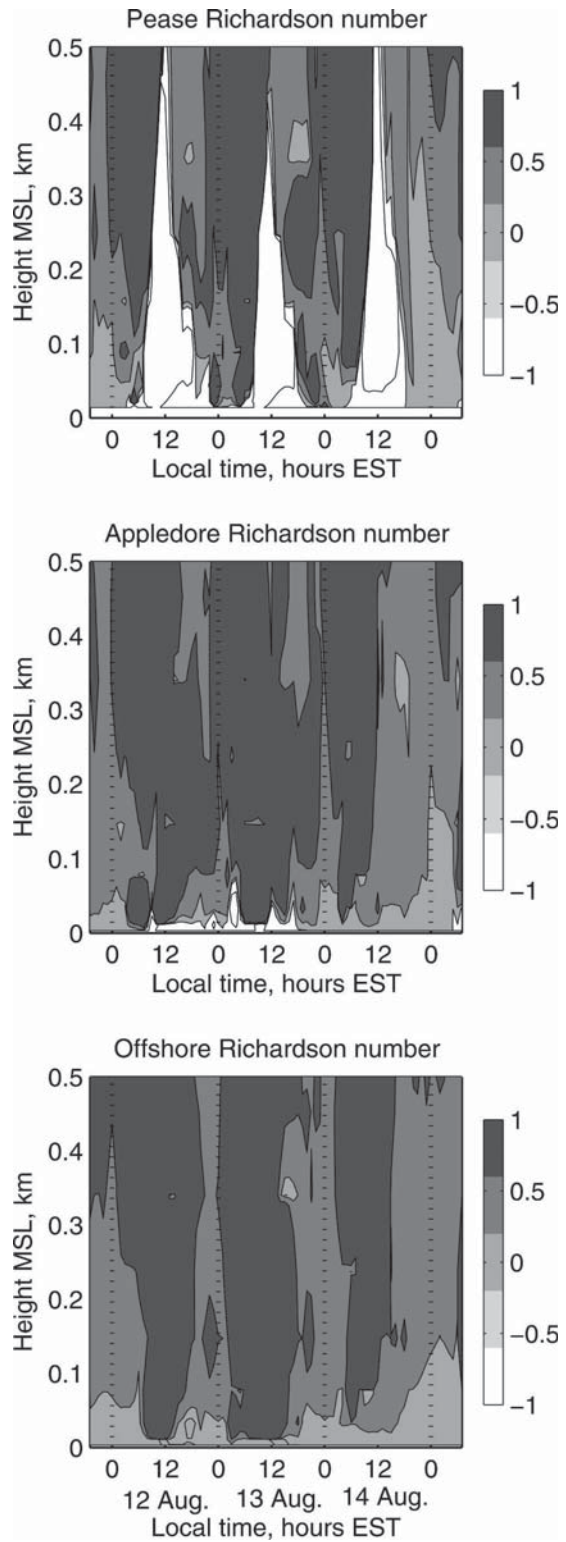


FIG. 13. Time–height cross sections of model Richardson number for 11–14 Aug over Pease, Appledore, and the offshore point.

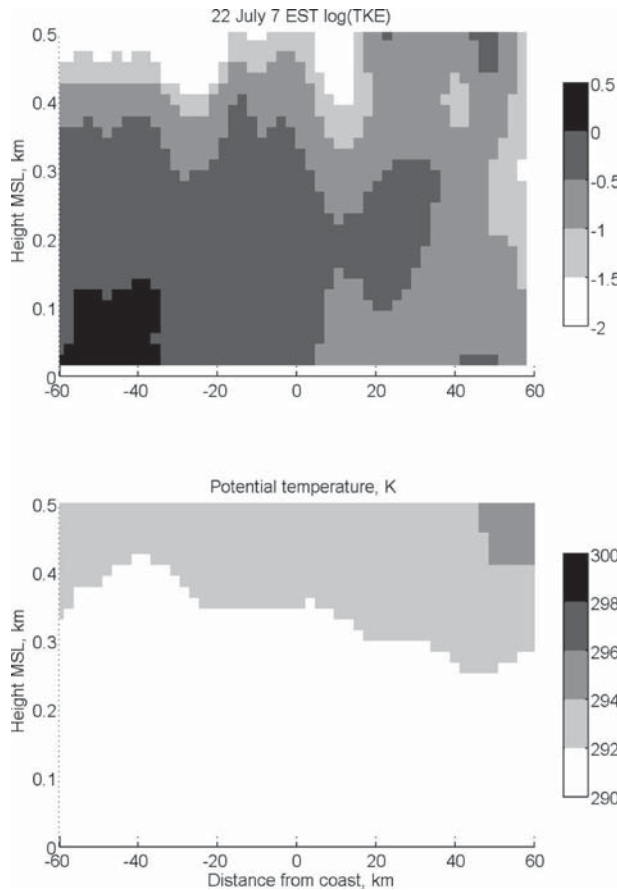


FIG. 14. TKE and potential temperature vertical cross sections at 0700 LST 22 Jul along the approximate wind direction (diagonal line in Fig. 1).

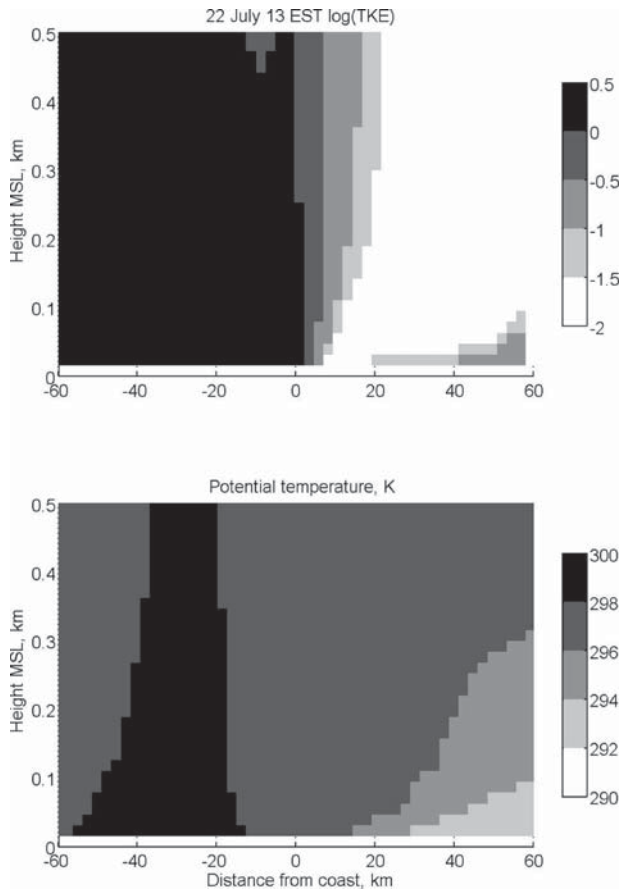


FIG. 15. TKE and potential temperature vertical cross sections at 1300 LST 22 Jul along the approximate wind direction (diagonal line in Fig. 1).

22 July. The plots are vertical cross sections along the approximate wind direction, which is shown as the diagonal line in Fig. 1. The coastline is at the zero point on the horizontal axis. In the early morning (Fig. 14) the temperatures of the land and sea are nearly equal and there is little horizontal gradient below 400 m. Weak turbulence is present over the land at low levels, decreasing rapidly with height. After crossing the coast, the turbulence decreases substantially (note the log scale of TKE), then increases again in a shallow layer near the surface. At midday (Fig. 15), the land is warm and there is a strong horizontal gradient of temperature in the lower levels. TKE decreases very rapidly as the air crosses the coast, and recovers slightly after traveling farther offshore.

5. Tracer results

Plots of the tracer plumes from COAMPS are a powerful tool for visualizing the transport phenomena. We show plots of tracer concentration (m^{-3}) with arbitrary

contours, keeping in mind that we are looking for general patterns rather than quantitative comparisons. Figure 16 shows the tracer from Boston in the morning of 22 July from the high-resolution run (2.5-km grid). The tracer emitted from Boston has been blown to the northeast after leaving the land at Cape Ann. Having been emitted into the nocturnal boundary layer, the plume is less than 300 m deep. It does not come ashore again within the 2.5-km domain. Later in the day (Fig. 17), the plume is deeper, up to 800 m, and therefore less concentrated. At the surface, it is very narrow because of the near-coastal convergence. It precisely hits the Isles of Shoals. At a higher level, the plume has moved more to the east. This type of wind shear with height was very common during the southwesterly flow.

The Boston tracer plume in the morning of 13 August (Fig. 18) looks rather similar to that on 22 July, except that it is slightly farther south. In the afternoon, however, the sea breeze has pushed the low-level plume inland along the New Hampshire and southern Maine coast (Fig. 19). The plume is somewhat broken

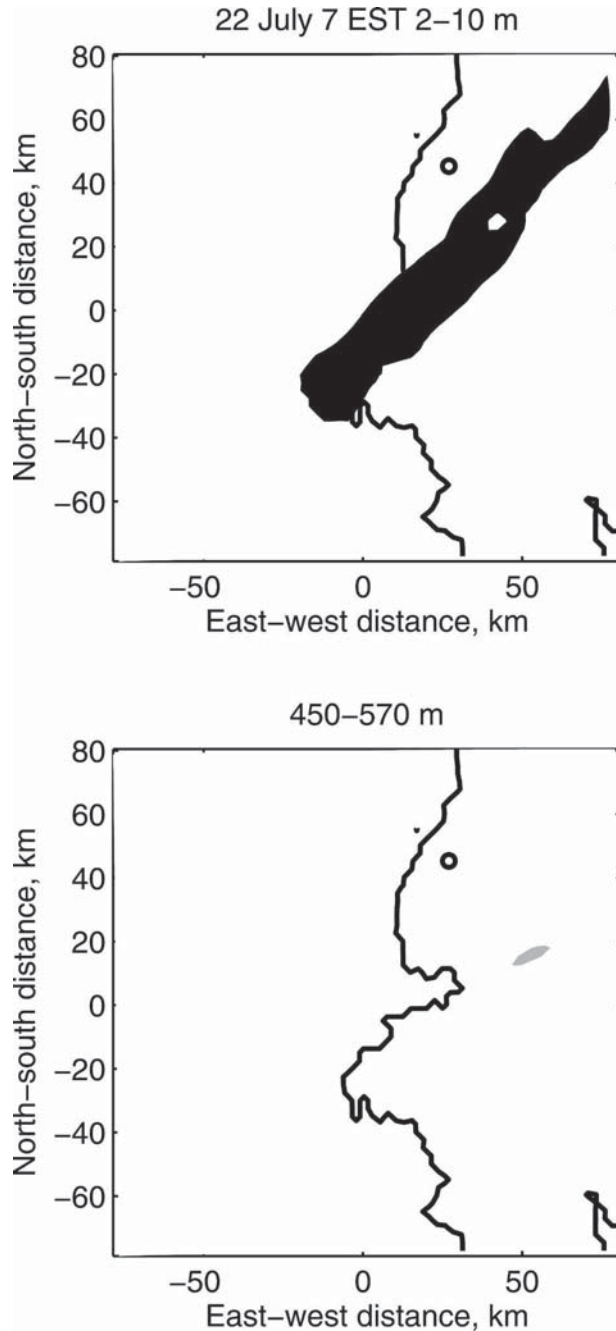


FIG. 16. Tracer plume from Boston at 0700 LST 22 Jul (arbitrary contours same for Figs. 16–19) for the two heights indicated.

by variations in the wind and in vertical mixing. At this resolution, COAMPS directly simulates some small areas of convection. The elevated plume is still headed to the northeast. Patterns on 12 and 14 August are roughly similar, but the sea breeze and therefore the tracer plume do not penetrate as far inland on the 14th. Note that the tracer plumes should not be interpreted as trajectories; in fact, the trajectories of air reaching

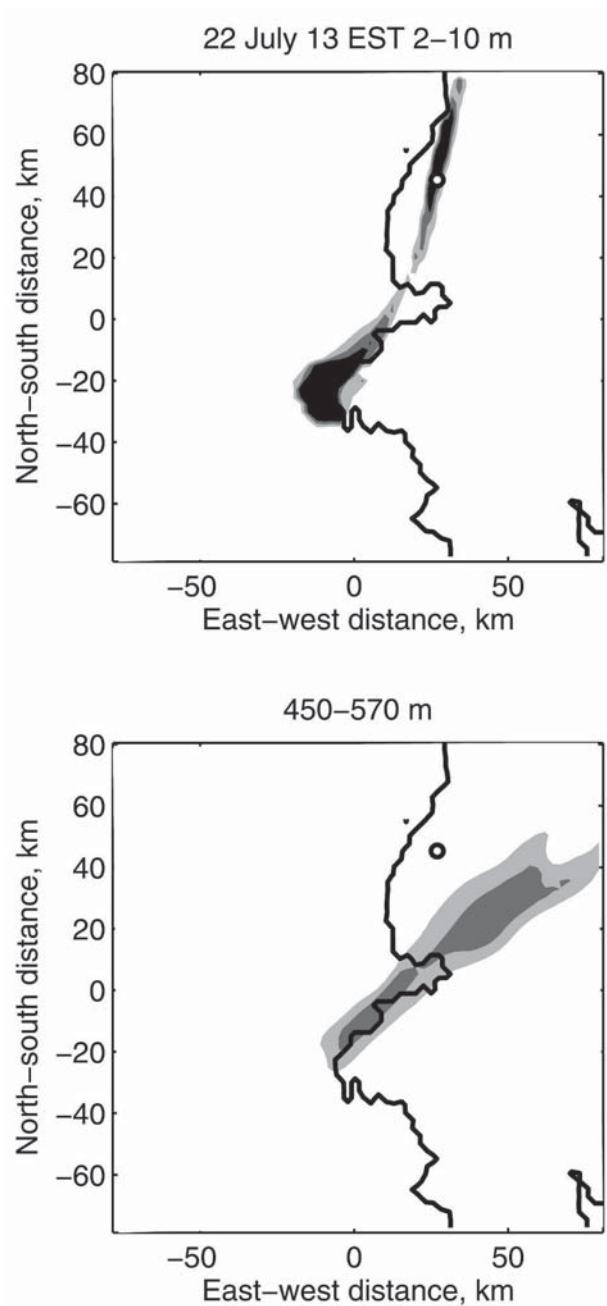


FIG. 17. As in Fig. 16, but at 1300 LST 22 Jul.

Thompson Farm (Durham, New Hampshire) at the surface go from Boston out to sea, then turn and come inland on the sea breeze. An example back trajectory is shown in Fig. 20.

The most similar chemical compound to a passive tracer is carbon monoxide (CO), which is emitted in urban areas and has a long lifetime. The measured CO mixing ratio at the Thompson Farm site is shown along with the modeled Boston tracer on the 2.5-km grid in

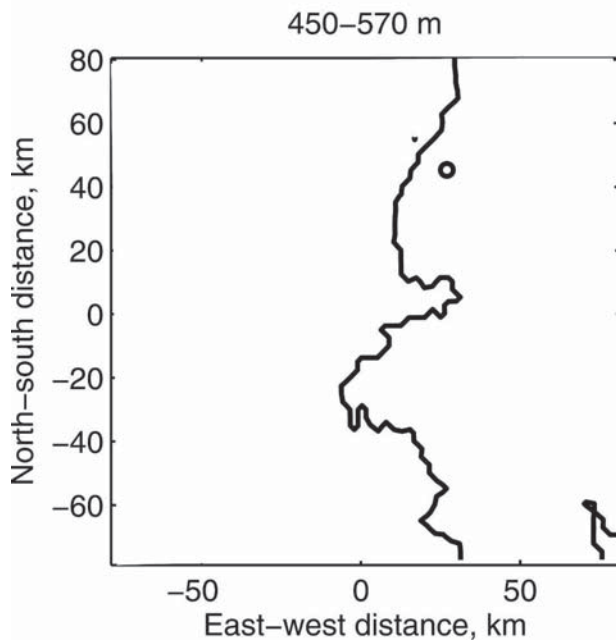
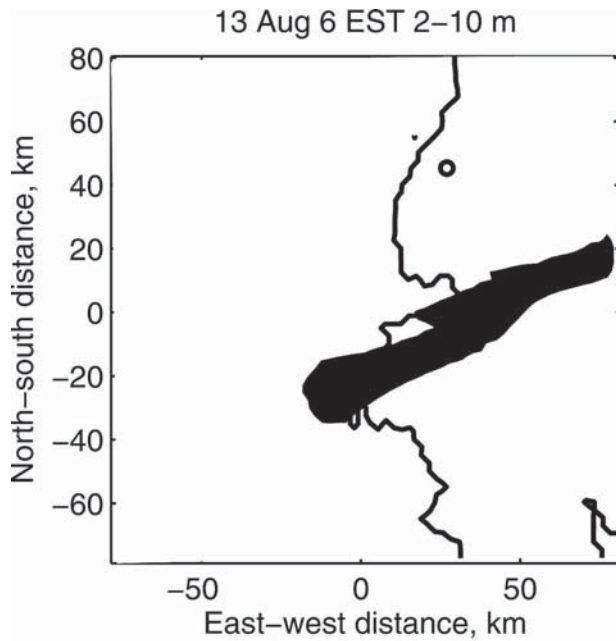


FIG. 18. As in Fig. 16, but at 0600 LST 13 Aug.

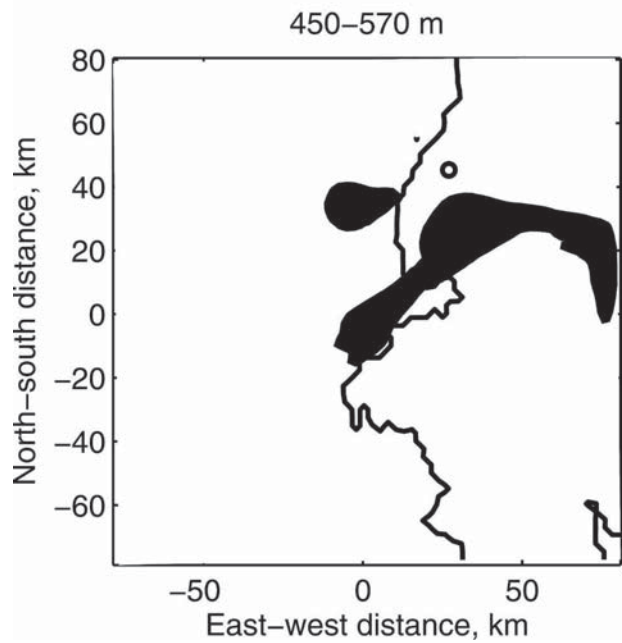
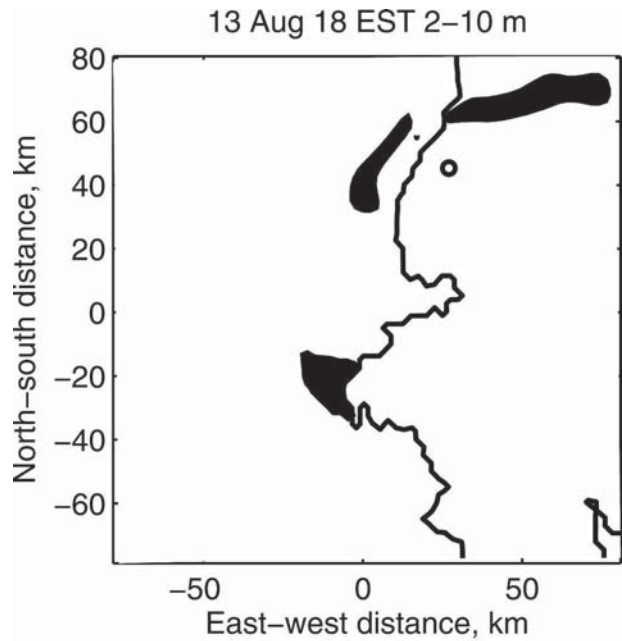


FIG. 19. As in Fig. 16, but at 1800 EST 13 Aug.

Fig. 21. Thompson Farm is located at 43.11°N , 290.05°E , approximately 15 km inland from the coast (see Fig. 1). We do not expect quantitative agreement between the tracer and measured CO, but we can make general comparisons. There are some rough similarities between the measurement and the modeled tracer, but also notable differences. On 12 August, the tracer peaks in the early evening when the sea-breeze front

reaches the site. The corresponding peak in the measured CO occurs about 2 h earlier. The modeled tracer peak is sharp and is followed by a decrease to more moderate levels, while the measured CO continues strong until the next morning. On 13 August, the modeled peak is extremely sharp, and is again delayed by several hours. The extended period of strong observed CO is again only partially captured by the modeled

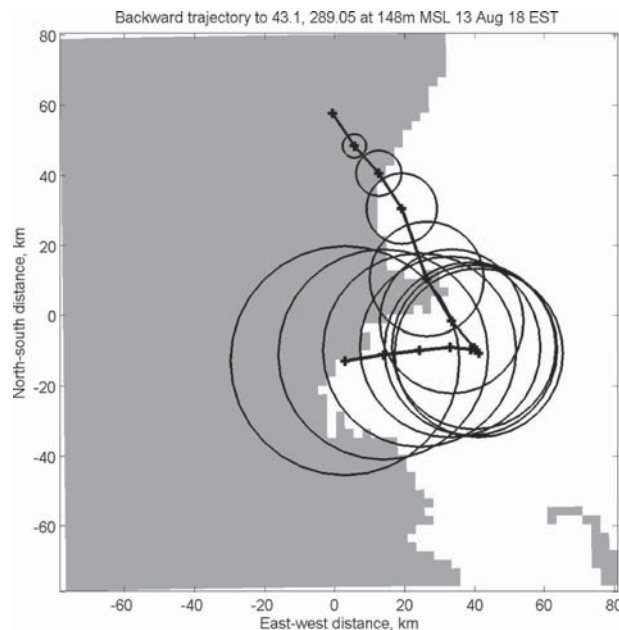


FIG. 20. Backward trajectory from Thompson Farm computed from the 2.5-km model winds. The trajectory ends at 1800 LST 13 Aug and goes back 12 h. The circles are a rough estimate of the uncertainty of the trajectory (30% of the travel distance). No vertical motion is considered in the computation of this trajectory.

Boston tracer. A side view from the south of the tracer plume at 1800 LST 13 August after the inland penetration of the sea breeze has stalled is shown in Fig. 22. The sea-breeze layer is 300–400 m deep. The cool sea-breeze layer has apparently not been subject to deep convective mixing while moving inland over the warm land, probably because it came inland late in the day. On 14 August, the most polluted day of the episode, the model misses the peak entirely because the simulated

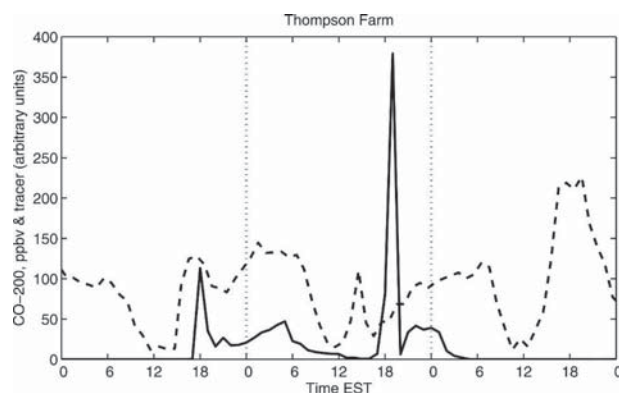


FIG. 21. Tracer from Boston (solid) compared with CO at the Thompson Farm site (dashed) on 12–14 Aug. The tracer is averaged over the lowest three model levels (approximately 0–90 m AGL) and arbitrarily scaled. Carbon monoxide is shown with 200 ppbv, a rough estimate of the regional background, subtracted.

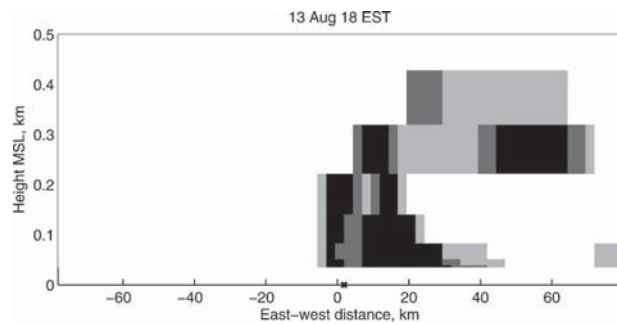


FIG. 22. Vertical east–west cross section of tracer plume from Boston at 1800 LST 13 Aug. Color scale is arbitrary. Cross section is taken at the latitude of Thompson Farm, the longitudinal position of which is shown by the X (near zero on the horizontal axis).

sea breeze does not penetrate far enough inland. Angevine et al. (2004) discuss the observations of this episode in more detail.

One possible reason, other than the previously discussed differences in wind direction, for the discrepancies between the modeled tracer and observed CO in Fig. 21 is that only Boston is considered. The 7.5-km grid was used with tracers from NYC and Boston, so we can examine whether some of the observed CO was coming from the NYC area. The 7.5-km grid run does have slightly different flow patterns as well. On 12 August, tracer from both sources reaches Thompson Farm in the 7.5-km run with a similar pattern to that shown in Fig. 21. The afternoon peak on 13 August is entirely from Boston, but there is a peak at night from NYC. The 7.5-km run does a better job with the large peak on 14 August, which has contributions from both Boston and NYC. Coarser resolution is often an advantage in comparisons with point observations.

At the 7.5-km grid spacing, the model domain is large enough to include both New York City, an important source region, and Acadia National Park, a receptor site of great interest. This allows us to say something about the relative importance of sources other than Boston, and to further explore some of the phenomena observed at Acadia (44.4°N, 291.8°E).

At 1300 LST 23 July, the plume from Boston on the 7.5-km grid (Fig. 23) looks rather similar to that on the 2.5-km grid on the previous day (Fig. 17). In the larger domain, however, we can see that the plume impacts the Maine coast at the surface, roughly corresponding to the observed ozone mixing ratios (Angevine et al. 2004). However, the NYC plume is also over Boston and impacts the Maine coast, both at the surface and aloft. If ozone and its precursors were as passive as our tracer, we would say that the model indicates similar pollution impact from NYC and Boston. However, the

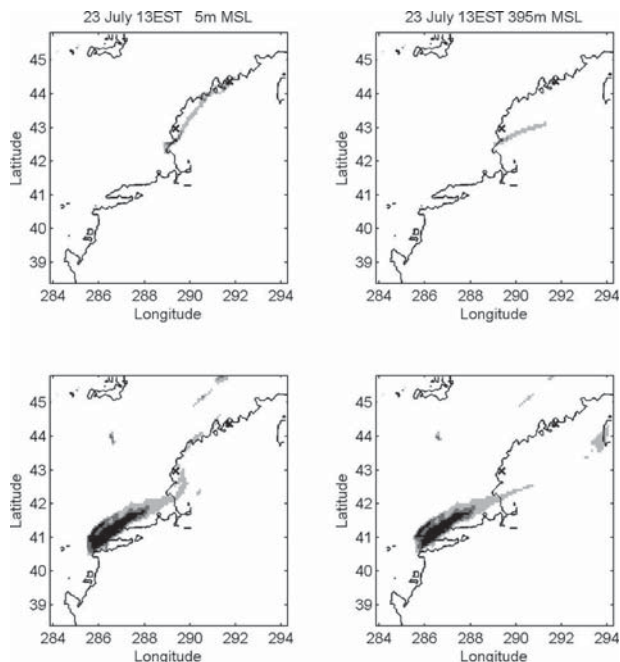


FIG. 23. Tracer concentrations on the 7.5-km grid at 1300 LST 23 Jul at (left) 5 and (right) 395 m MSL for the (top) Boston and (bottom) New York City tracer. Shading scale is arbitrary but identical for all panels of this figure and Fig. 24. Appledore Island and Acadia National Park are marked with X.

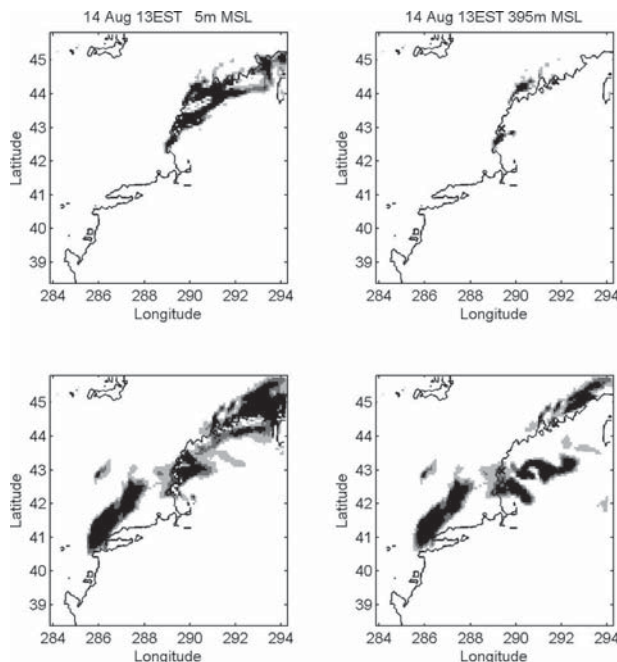


FIG. 24. Tracer concentrations on the 7.5-km grid at 1300 LST 14 Aug at (left) 5 and (right) 395 m MSL for (top) Boston and (bottom) New York City tracer. Shading scale is arbitrary but identical for all panels of this figure and Fig. 23. Appledore Island and Acadia National Park are marked with X.

NYC plume has traveled a considerable distance over land, and has certainly been subject to considerable deposition of ozone and precursors to leaf surfaces. At higher levels, both plumes have traveled to the northeast, and the NYC plume from the previous day has reached Nova Scotia.

At 1300 LST 14 August, the situation (Fig. 24) is different in ways that are consistent with the lighter and more variable winds described above. The concentrations show the integrated effects of several days. The tracers from both sources combine to produce high concentrations along the entire coast. The plume is patchy because the effects of successive coastal convergences, resulting from each day's sea breeze, are advected up the coast. There is some impact aloft on the Acadia National Park vicinity from Boston. Aloft, pieces of the NYC plume are over the Gulf of Maine between Boston and Nova Scotia, but also appear over coastal Maine, including Acadia National Park. The Boston plume has less impact aloft, because there is less of it (more tracer is released over NYC than over Boston), but also because the NYC tracer is mixed vertically over land on more than one day.

Angevine et al. (2004) noted peaks of ozone at night at Cadillac Mountain, a high-elevation site in Acadia National Park. Considerably less ozone was observed at

sites nearer sea level. The model provides some insight into the processes leading to those peaks. Late on 14 August (1900–2300 LST), the model shows some impact from both Boston and New York City at the approximate elevation of Cadillac Mountain (466 m ASL). Late on 13 August, another time with a strong ozone peak at Cadillac Mountain, both Boston and NYC plumes impact the Acadia vicinity strongly at the surface, but only Boston has any influence aloft, and that is relatively weak.

6. Discussion and conclusions

Our COAMPS model runs reproduced the real observed atmosphere more than well enough to show the most important features, even though this is far from a typically simple test case. The first conclusion, then, is that a mesoscale numerical modeling system can be a useful tool for understanding complex small-scaled situations. This is important because it allows for an extension of the model use; model output can now be used to complement observational results in studying particular processes or cases. The model can then provide more complete and fully consistent four-dimensional information in a way that is not possible to obtain from a field experiment alone. In this study, the implementa-

tion strategy includes using analyzed lateral boundaries as the only external dynamic constraint. This safeguards the realistic representation of the larger-scale meteorological setting and also means that model error growth is controlled. The high-resolution detail is provided entirely by the mesoscale model, allowing it to develop its own internal dynamics and internal balance between different processes. There are, however, still some differences between the simulation results and reality that must be acknowledged.

The most important difference is the lack of sufficient stability in the modeled offshore profiles. The model has a tendency to produce a near-neutral layer at the surface over the water, which is not observed. This is probably caused by too much vertical mixing in the model boundary layer formulation, a common problem in modeling of stable boundary layers. More specifically, it must indicate too much mixing among the lowest levels of the atmosphere in the model, and too little heat flux into the model surface. This could have some effect on the modeled dispersion, but we have no means to isolate its effect from others.

The modeled winds differ more from reality at some times than others. The most important discrepancy here is the lack of penetration of the sea breeze on 14 August. In reality, the sea breeze probably penetrated only a little farther than the measurement site at Thompson Farm. Because of the strong gradient across the sea-breeze front, a small discrepancy in the penetration distance (of the order of the grid spacing) makes a large difference in the modeled tracer concentration. It is unreasonable to expect a model to reproduce point measurements under conditions like these.

There is no obvious degradation in the performance of the model at the coarser 7.5-km grid spacing relative to the finer 2.5-km grid. In fact, in the tracer comparisons at Thompson Farm, the 7.5-km results were arguably better. This is a well-known effect in comparisons with point measurements. The more precise results from a higher-resolution model, because they have stronger gradients and more structure, are likely to have the right concentrations in the (perhaps only slightly) wrong places, while the broader brush strokes of the coarser model are more likely to get things about right (but with weaker variations).

Observations to compare with the modeled plume structures are sparse. Most routine air quality monitoring sites measure only ozone, which has a very strong diurnal cycle that makes using it to diagnose transport extremely problematic. The few point measurements of CO are somewhat more useful. The shipboard lidar observations of ozone profiles in the July case are

roughly consistent with what was modeled (see Angevine et al. 2004, Figs. 9 and 10).

From the narrowness of the modeled tracer plumes, we can see that wind direction in the model is critical, both to comparisons with point measurements and to any examination of longer-range transport. A few degrees of error in wind direction will cause the narrow plumes to miss particular receptors entirely. In reality, the source regions are not as sharp edged as in the model, and therefore the plumes are also broader and fuzzier.

How is our picture of reality changed or confirmed by these results? What have we learned *from* the modeling, as distinct from what we have learned *about* the modeling?

We started with a number of questions about the formation of the stable internal boundary layer (IBL) over the water and the fate of the air above that layer. It seems clear that the formation of the IBL in the model is limited by the resolution and physics of the model. In other words, the change in surface heat flux and roughness, at least during the day, is so rapid that the model responds as quickly (or in as short a distance) as it can, but that is still not as quickly as reality. Newer observations (Angevine et al. 2005) suggest that the IBL forms very quickly in the first few kilometers offshore, so a model with a resolution finer than a kilometer would likely be required to reproduce that process.

When viewed from far downwind (e.g., Angevine et al. 1996), directional shear and differential advection resulting from stability offshore result in distinct layering in the vertical. Closer examination of the processes near the coast, however, shows a more continuous process. The daytime continental boundary layer, about 1.5 km deep and heavily polluted, does shear out after crossing the coast, and air at different levels goes different directions at different speeds. The lowest layer (surface to 200–500 m) remains at the surface and is strongly cooled while keeping its chemical contents. At night, this is the only polluted layer. When a higher, polluted layer exists during the day, it also becomes isolated after crossing the coast, so it shears out and transports its pollutants, nearly without losses, in a different direction than that of the lower layer. When a sea breeze pushes the lowest layer inland, as in the August case we have discussed, a vertical profile over the water may show a clean layer below a polluted layer.

The plume structures produced in our tracer experiments are sometimes relatively simple and sometimes quite complex. When the wind speed and direction are roughly constant, as in the July case, the tracer advects downwind as a coherent plume at the surface, mean-

dering back and forth as the wind direction changes through a narrow range. When the background wind is weaker, as in the August case, the plume is broken up into segments that move in diverse ways. In either case, the increased height of daytime mixing produces pulses of tracer at higher levels (500–1500 m) that tend to be advected in a consistent direction during the entire episode. Pollutants from sources farther upwind of the coast behave in an even more complex fashion, being subject to possibly more than one diurnal cycle over land.

One of the most interesting observations we had hoped to elucidate with the model is the nocturnal ozone peaks at Cadillac Mountain in Acadia National Park (Angevine et al. 2004, their Fig. 16). The modeled tracer does impact the vicinity aloft on the night of 14 August, but not on the previous night. The model does not show the kind of direct, unambiguous transport aloft that had been hypothesized. However, the modeled tracer is released discretely over a limited area and there is a significant transport of tracer along the whole coast in the 7.5-km nest, at least in the August case shown here. It is likely that a more realistically widespread distribution of emissions would cause a less distinct tracer concentration pattern and more continuously high concentrations around Acadia National Park, at least in some conditions. It therefore seems clear that the model provides some support for the hypothesis that observed elevated concentrations of pollutants at Acadia National Park are transported from the Boston and New York metropolitan areas.

Lofting, defined as the transport of polluted layers along potential temperature surfaces, and therefore away from the cooler water surface, is not directly seen in the model. Instead, the low-level vertical mixing remains sufficient to keep the plume attached to the surface in offshore flows. Although the model low-level mixing is too intense, the result is consistent with Angevine et al. (2004), who concluded that lofting was not needed as an explanation for the observed structure in these cases. Whether or not a sea breeze is present, an assumption of isentropic transport (e.g., Angevine et al. 1996; Dye et al. 1995), while perhaps not unreasonable for analysis of longer-range transport, is too simple in the short- to medium-range context. Considerable vertical transport and mixing are likely results of the vertical velocities in the sea-breeze frontal zones and to substantial wind shear atop the sea breeze.

We cannot draw firm conclusions about the formation of a mixed layer downwind from these results, because the model mixes too much in the vertical even near shore. Different modeling techniques will be needed to further elucidate this matter.

The modeled sea breeze is strongly affected by the coastline geometry and divides into two almost separate systems in the two bays resolved by the innermost domain. In both cases, the wind speed has a maximum along the southern shore of the bay, being accelerated by a cross-coast mesoscale pressure gradient generated by the land–sea temperature contrast. Conversely, the strongest daytime offshore flow for the case where no sea breeze formed are found along the northern portion of each bay, also having the warmest low-level air “to the left” in the flow direction.

The offshore flow on top of the sea breeze is unexpectedly strong and shallow, only about 2 times the depth of the sea breeze itself, and about 2 times as strong as the offshore flow in which it is embedded. It has the geometric appearance of a gravity wave, rather than that of a traditional sea-breeze return flow. Above this deeper layer of weak flow, there are also signs of a weak gravity wave tilting inland on top of the return flow, in both the horizontal and vertical winds and in the potential temperature. It is not clear if this feature is triggered by the upstream terrain, constructively interacting with the sea-breeze front to form this wave-like strong counterflow branch, or if the wave shape is directly a consequence of the strong up–down couplet in the vertical wind speed at the sea-breeze front.

As the sea breeze terminates, a strong offshore low-level jet appears at about the same height as the top of the previous sea breeze. This flow is several times stronger than the background offshore flow, and is present also in the case without a proper sea breeze but just a weak low-level offshore deceleration. We hypothesize that this is an inertial response triggered when the opposing sea-breeze pressure force collapses in the evening.

In the final analysis, in addition to the interesting and complex phenomena and structure we see in the model output, the basic conclusion is strengthened: major pollution episodes along the northern New England coast are caused by efficient transport of pollutants from distant sources. The transport is efficient because the stable marine boundary layer allows the polluted air masses or plumes to travel long distances with little dilution or chemical modification. The sea-breeze or diurnal modulation of the wind, and thermally driven convergence along the coast, modify the transport trajectories.

Acknowledgments. This work was begun while the first author was a short-term visitor at Stockholm University, sponsored by the International Meteorological Institute (IMI). The model calculations were performed at the Swedish National Supercomputer Centre

(NSC). Sounding data from the *Ronald H. Brown* were provided by Dan Wolfe of NOAA's Environmental Technology Laboratory.

REFERENCES

- Angevine, W. M., M. Trainer, S. A. McKeen, and C. M. Berkowitz, 1996: Mesoscale meteorology of the New England coast, Gulf of Maine, and Nova Scotia: Overview. *J. Geophys. Res.*, **101**, 28 893–28 902.
- , and Coauthors, 2004: Coastal boundary layer influence on pollutant transport in New England. *J. Appl. Meteor.*, **43**, 1425–1437.
- , J. E. Hare, C. W. Fairall, and D. E. Wolfe, 2005: Development of the coastal boundary layer in offshore flow from New England. Preprints, *Sixth Conf. on Coastal Atmospheric and Oceanic Prediction and Processes*, San Diego, CA, Amer. Meteor. Soc., CD-ROM, 5.4.
- Bott, A., 1989: A positive definite advection scheme obtained by nonlinear renormalization of the advective fluxes. *Mon. Wea. Rev.*, **117**, 1006–1015.
- , 1992: Monotone flux limitation in the area-preserving flux-form advection algorithm. *Mon. Wea. Rev.*, **120**, 2592–2602.
- Burk, S. D., and T. Haack, 2000: The dynamics of wave clouds upwind of coastal orography. *Mon. Wea. Rev.*, **128**, 1438–1455.
- , and W. T. Thompson, 2004: Mesoscale eddy formation and shock features associated with a coastally trapped disturbance. *Mon. Wea. Rev.*, **132**, 2204–2223.
- , T. Haack, L. T. Rogers, and L. J. Wagner, 2003: Island wake dynamics and wake influence on the evaporation duct and radar propagation. *J. Appl. Meteor.*, **42**, 349–367.
- Colby, F. P., Jr., 2004: Simulation of the New England sea breeze: The effect of grid spacing. *Wea. Forecasting*, **19**, 277–285.
- Cooper, O. R., and D. D. Parrish, 2004: Air pollution export from and import to North America: Experimental evidence. *Intercontinental Transport of Air Pollution*, A. Stohl, Ed., Vol. 4, Part G, *The Handbook of Environmental Chemistry*, Springer, 41–67.
- Davies, H. C., 1976: A lateral boundary formulation for multi-level prediction models. *Quart. J. Roy. Meteor. Soc.*, **102**, 405–418.
- Dorman, C. E., T. Holt, D. P. Rogers, and K. Edwards, 2000: Large-scale structure of the June–July 1996 marine boundary layer along California and Oregon. *Mon. Wea. Rev.*, **128**, 1632–1652.
- Dye, T. S., P. T. Roberts, and M. E. Korc, 1995: Observations of transport processes for ozone and ozone precursors during the 1991 Lake Michigan Ozone Study. *J. Appl. Meteor.*, **34**, 1877–1889.
- Estoque, M. A., 1961: A theoretical investigation of the sea breeze. *Quart. J. Roy. Meteor. Soc.*, **87**, 136–146.
- Fast, J. D., and W. E. Heilman, 2003: The effect of lake temperatures and emissions on ozone exposure in the western Great Lakes region. *J. Appl. Meteor.*, **42**, 1197–1217.
- Haack, T., S. D. Burk, C. Dorman, and D. Rogers, 2001: Super-critical flow interaction within the Cape Blanco–Cape Mendocino orographic complex. *Mon. Wea. Rev.*, **129**, 688–708.
- , —, and R. M. Hodur, 2005: U.S. West Coast surface heat fluxes, wind stress, and wind stress curl from a mesoscale model reanalysis. *Mon. Wea. Rev.*, **133**, 3202–3216.
- Hanna, S. R., and R. Yang, 2001: Evaluations of mesoscale models' simulations of near-surface winds, temperature gradients, and mixing depths. *J. Appl. Meteor.*, **40**, 1095–1104.
- Harshvardhan, R. Davies, D. Randall, and T. Corsetti, 1987: A fast radiation parameterization for atmospheric circulation models. *J. Geophys. Res.*, **92**, 1009–1015.
- Hodur, R. M., 1997: The Naval Research Laboratory's Coupled Ocean/Atmosphere Mesoscale Prediction System (COAMPS). *Mon. Wea. Rev.*, **125**, 1414–1430.
- Kain, J. S., and J. M. Fritsch, 1993: Convective parameterization for mesoscale models: The Kain–Fritsch scheme. *The Representation of Cumulus Convection in Numerical Models*, Meteor. Monogr., No. 46. Amer. Meteor. Soc., 165–170.
- Keen, C. S., and W. A. Lyons, 1978: Lake/land breeze circulations on the western shore of Lake Michigan. *J. Appl. Meteor.*, **17**, 1843–1855.
- Liu, M., D. L. Westphal, S. Wang, A. Shimizu, N. Sugimoto, J. Zhou, and Y. Chen, 2003: A high-resolution numerical study of the Asian dust storms of April 2001. *J. Geophys. Res.*, **108**, 8653, doi:10.1029/2002JD003178.
- Lyons, W. A., and L. E. Olsson, 1973: Detailed mesometeorological studies of air pollution dispersion in the Chicago lake breeze. *Mon. Wea. Rev.*, **101**, 387–403.
- , and H. S. Cole, 1976: Photochemical oxidant transport: Mesoscale lake breeze and synoptic-scale aspects. *J. Appl. Meteor.*, **15**, 733–743.
- Marshall, C. H., R. A. Pielke Sr., L. T. Stayaert, and D. A. Willard, 2004: The impact of anthropogenic land-cover change on the Florida sea breezes and warm season sensible weather. *Mon. Wea. Rev.*, **132**, 28–52.
- Mellor, G., and T. Yamada, 1974: A hierarchy of turbulence closure models for planetary boundary layers. *J. Atmos. Sci.*, **31**, 1791–1806.
- Nachamkin, J. E., 2004: Mesoscale verification using meteorological composites. *Mon. Wea. Rev.*, **132**, 941–955.
- Rutledge, S. A., and P. V. Hobbs, 1983: The mesoscale and microscale structure of organization of clouds and precipitation in midlatitude cyclones. VIII: A model for the “seeder-feeder” process in warm-frontal rainbands. *J. Atmos. Sci.*, **40**, 1185–1206.
- Shi, J. J., S. W. Chang, T. R. Holt, T. F. Hogan, and D. L. Westphal, 2004: A meteorological reanalysis for the 1991 Gulf War. *Mon. Wea. Rev.*, **132**, 623–640.
- Sillman, S., P. J. Samson, and J. M. Masters, 1993: Ozone production and urban plumes transported over water: Photochemical model and case studies in the northeastern and midwestern United States. *J. Geophys. Res.*, **98**, 12 687–12 699.
- Skyllingstad, E. D., R. M. Samelson, L. Mahrt, and P. Barbour, 2005: A numerical modeling study of warm offshore flow over cool water. *Mon. Wea. Rev.*, **133**, 345–361.